AAPG Annual Convention
Salt Lake City, Utah
May 11-14, 2003

Seismic-Based Geomechaical Modeling Provides Attributes for Directional Well Planning

EVGENII KOZLOV, Paradigm Geophysical, Moscow, Russia; IGOR GARAGASH, United Institute of Earth Physics, Moscow, Russia; ALLEN LOWRIE, Consultant, Picayune, MS.

Abstract
Apart of geostructure, routinely delivered by 3D seismic, estimates of pore pressure, rock fracturing, and triaxial stress are needed for efficient directional well planning. We show how 3D distributions of these parameters can be mapped by azimuthal analysis of seismic interval velocity and angle of incidence dependent reflectivity combined with geomechanical modeling. The latter is based on the use of seismic-derived 3-D distribution of the rock elastic moduli, angles of internal friction, rock cohesion, and plastic relaxation constants. Considering the fluid-saturated rocks as an undrained anisotropic elasto-plastic medium subjected to lithostatic and tectonic stresses, and applying a fast Lagrangean code formalism for numerical geomechanical modeling, 3D cubes of expected pore pressure, intensity of fracturing caused by shear strains, and parameters of principal horizontal components of the stress are created for the area studied – a Middle Priob'e's oil field in West Siberia.

Introduction
Estimation of the stress state and fluidodynamics using seismic data had proved to enhance interpretation of seismic data in search for oil and gas in both regional (subsalt Gulf of Mexico sediments) and local seismic field scale (tight Paleozoic carbonates and Mesozoic sandstones of Volgo-Ural, East and West Siberia regions), Baransky and Komov, 1986; Kozlov et al., 2000; Mushin et al., 2000. The well known elastic earth model subject to confining and tectonic stresses (Cundall, 1988, Garagash et al., 1994) was implemented to define zones of relative decompaction and maximum principal tangential strains as potential agents of fracturing. The results obtained were used as valuable attributes for integrated reservoir characterization and helped understand the hydrocarbon deposits origin and evolution.

Relative decompaction and concentration of tangential strains, however, do not describe directly the rock properties directly related to directional well planning. To expand the range of the modeling capabilities, we replaced the isotropic elastic earth model by anisotropic elasto-plastic one and elaborated a technique for definition of an additional set of mechanical parameters allowing prediction of minimum and maximum horizontal stresses, aligned fracturing intensity and orientation, and pore pressure. Testing the newly developed 3D geomechanical modeling technique combined with azimuthal analysis of seismic velocity and reflectivity provided for creation of a 3D Earth model that can be effectively used for planning optimum well trajectories, casing, and drilling regime including mud weight variation.

Input data
Basic set of input data is represented by spatial distribution of rock density and anisotropic elastic moduli deduced from geologic structure and anisotropic depth velocity model. The latter is created using prestack depth migration of seismic data and high resolution residual moveout analysis (Kozlov and Varivoda, 2003).

To provide for definition of an additional set of rock mechanics parameters including strain and shear strength (cohesion) limits, dilation angles, internal friction angles, and upper limits of the pore fluid pressure, the detailed lithology variations in main stratigraphic plays of the Moddle Priob'e's field and its internal structure were mapped using sequence stratigraphy studies, azimuthal velocity and AVO analysis, and amplitude inversion.

Elasto-plastic anisotropic model of porous fluid saturated rock
The key idea is that real rock subjected to confining and/or tectonic stresses usually deforms as elasto-plastic medium: at small stresses and strains, the rock deforms as an elastic body, but past the maximum of the stress-strain curve, when the rock strength limit is reached, the rock reacts to stress as a *plastic* medium, especially at high saturation. At this

segment of the stress-strain curve, deformation continues to increase with *decreasing* stress, the gradient of the decrease depends on the degree of anelasticity and the properties of pore fluid. Also, for this segment of the stress-strain curve, development of fractures and fault-like deformations is characteristic. When minimum and maximum horizontal stresses differ essentially, orientated fracturing is developed, the fracture planes tending to be normal to minimum horizontal stress. As a result, the rock moduli, and consequently, seismic velocities become anisotropic. Taking into account the role of vertical azimuthally orientated fracturing as the main agent of increased reservoir permeability, of primary interest is lateral variation of the minimum horizontal stress magnitude and direction governing the fracturing generation and evolution.

Forming of a particular pattern of fracturing depends on the distribution of rockmass inhomogeneities and the shapes of formation boundaries, while the distribution of zones of increased fracturing is controlled by the variations of the internal friction angles, and sliding along fault surfaces results in permeability-dependent re-distribution of pore pressure.

These notions are inherent in the anisotropic elasto-plastic rock model developed for enhanced geomechanical simulations.

Real data example

Seismic data. On the oil field chosen for the new geomechanical model testing (**Figure 1**), the sedimentary cover is represented by siliciclastic rocks of moderate compaction. The target oil reservoirs are located in the interval between seismic horizons **B** (Upper Jurassic shale) and **T2** (about 300 m above the Pre-Jurassic basement, marked as Horizon **A** in **Figure 2**). The interval is penetrated by horizontal and vertical fractures. The horizontal fractures are attributed to the boundaries between reservoir rocks (tight sandstones) and shaly layers, while vertical fracturing is assumed to be genetically tied up with a series of nearly parallel small amplitude faults penetrating all the interval between horizons **B** and **A.**

High resolution azimuthal velocity and AVO analysis revealed no essential anisotropy above the horizon B, while the rockmass below **B** proved to be distinctly anisotropic**, Figures 3 – 5**.

Assuming the rocks in the interval between seismic horizons B and T2 can be horizontally transversely isotropic (HTI model) due to azimuthally aligned vertical fracturing, the interval velocities are calculated in directions normal (**Figure 3a**) and parallel (**Figure 3b**) to the HTI axis of symmetry (**Figure 4a**), i.e., parallel and normal to the vertical fracturing strike. As seen, velocities in these mutually orthogonal directions differ from each other quite significantly: the HTI anisotropy coefficient δ, defined with respect to the vertical, reaches – 0.18, **Figure 4b**. (For zero anisotropy, δ = 0). Hence, the fracturing in the target interval is quite intense and rather distinctly aligned along certain azimuths, varying over the oil field area. Note increased anisotropy (i.e., increased vertical fracturing) in the area of high productivity wells 1, 2, 4, and 6, and dominantly N-S orientation of fracture strikes in this area, while in general, NNW – SSE orientation of fractures is characteristic for the field area, **Figure 4a.**

The NNW – SSE direction is also the dominant orientation of the faulting strikes, **Figure 1**.

Azimuthal AVO analysis is carried out for the same azimuthal segments as velocity analysis. Asimuthal AVO gradient maps created for horizon T1 (situated between horizons B and T2, just at the base of the oil reservoir, **Figure 2**), also reflect essential anisotropy within the reservoir, **Figure 5**. In contrast to interval velocity maps related to rather thick interval (about 300 m), the reflectivity anisotropy, revealed by azimuthal AVO analysis, relates to a very thin interval immediately above the reflector T1 (i.e., relates directly to the oil reservoir). Despite the difference, results of azimuthal velocity and AVO analyses are visually alike, hence, the target interval between horizons B and T2, including horizon T1 (see **Figure 2**), can be considered as vertically homogeneous with relation to HTI anisotropy parameters. Average anisotropy coefficient δ in the high productivity area derived from the AVO azimuthal analysis data is about - 0.13.

Geomechanical modeling results. Geostructure, seismic velocity values and its anisotropy, along with borehole data on spatial variations of rock density and lithology, allowed to create a 3D cube, where each cell contains a set of parameters: bulk and shear anisotropic elastic moduli, density, angle of internal friction, rock cohesion, strength limit, and initial distribution of stresses defined by geologic structure. From these data, using the model described above, a set of geomechanical parameters needed for efficient planning of a directional well trajectory, casing design, and drilling regime including mud weight control, is defined at the cube cells. The set includes:

- Tri-axial stress values;
- Pore pressure;
- Fracturing intensity and orientation.

Since the image of the cube is not quite self-explanatory (see, e.g., the distribution of average principal stress, **Figure 6**), spatial variation of these parameters is illustrated by a series of profiles, maps, and interval cubes cut from the general cube, **Figures 7–10.**

Vertical profiles of pore pressure and lithostatic stress components calculated using the anisotropic elasto-plastic rock model see in **Figure 7.** Small, and in the target interval – negative difference between minimum horizontal component of lithostatic stress and pore pressure causes weak resistivity of the reservoir rocks to extensional fracturing.

Magnitude and orientation of minimum horizontal stress in stratigraphis plays above horizon B differs essentially from those in the target interval (between horizons B and T2), **Figure 8**. Note much more intense horizontal stresses in the target interval and general consistence between strikes of main faults (**Figure 1**), orientations of the HTI axis of symmetry (**Figure 4a**), and orientations of minimum horizontal stresses in the target interval, **Figure 8b**: in the area of high productivity, orientation of all these features is N-S, while in the areas of intense faulting, the NNW-SSE and ENE-WSW orientation prevails. Also, the area of high productivity is marked with the increased difference between minimum and maximum horizontal stresses (**Figure 8b**), and with the increased HTI anisotropy (**Figures 4b** and **5**).

Maps of fracture intensity and lateral pore pressure variations in the target interval calculated using the new model are shown in **Figures 9** and **10**, respectively.

The cube front facet *y* = 3000 m (**Figures 9** and **10**) cuts the middle of the anticline in latitudinal direction. As seen, the target interval is characterised by increased fracturing (**Figure 9b**) marked by increased HTI anisotropy, **Figures 4** and **5**. The zone of maximum fracturing within the target interval is attributed to the south-east flank of the local uplift in Pre-Jurassic basement. The uplift is interpreted to have created the zone of increased vertical component of confining stress (not shown here). **Figures 8b** and **9a** considered together with the data on HTI anisotropy (**Figures 4** and **5**) provide a detailed picture of fracturing orientation and intensity.

The pore pressure within the target interval (**Figures 7** and **10a**) is higher than in the enclosing strata, and exceeds hydrostatic pressure by several tens of percent, while in the pore pressure map (**Figure 10b**), minimum to maximum pressure relation is insignificant (about 0.9).

Tied up to the existing geostructural carcass, the geomechanical modeling results represented by cubes of tri-axial stress and pore pressure, along with the intensity and orientation of vertical azimuthally aligned fracturing, provide database sufficient to properly navigate directional well trajectory, design well casing, and adjust mud weight in the course of drilling.

The technique above is supported by a series of modern software products of Paradigm Geophysical, BV., and a fast Lagrangean code modeling system of Itaska.

Conclusion

• New developments in azimuthal velocity and AVO analysis facilitate transfer from isotropic elastic to seismic-based anisotropic elasto-plastic Earth model. This expands the capabilities of geomechanical modeling as a tool for enhanced reservoir characterization and directional borehole planning in unevenly stressed, faulted and fractured reservoirs by a detailed 3D mapping of the fracturing and pore pressure in addition to accurate prediction of the rock stressed state.

• In the oil field under study, the geomechanical modeling-derived lateral variations of minimum horizontal stress, fracturing parameters, and spatial (3D) variations of pore pressure, provide a valuable information for reservoir simulation, as well as for well casing design and mud weight adjustment in the course of drilling..

References

Baransky N.L., Komov D.A., 1986, Theoretical seismograms for plane models with account for the state of stress, in: Enhancement of exploration and prospecting in Ural region, Sverdlovsk, 99-100, In Russian.

Cundall P.A., 1988. A microcomputer program for modelling large-strain plasticity problem. Numerical methods in Geomechanics. Balkema, Rotterdam, 2101-2108.

Garagash I.A., Nikolaevsky V.N., Shatilov V.I., 1994. Connection of the deep anomalies of the crust stresses with under salt hydrocarbon deposits of the North Caspian. Proceedings of the RAS, **338**, 383- 386.

Kozlov, E.A., Garagash I.A., Mushin I A., Makarov V.V., and Lowrie A., 2000. Seismic-based Geomechanical Restorations in Volgo-Ural Region and Offshore Louisiana. EAGE 62nd Conference and Technical Exhibition, Glasgow, P-111.

Kozlov and Varivoda, 2003, Dense 3D Residual Moveout Analysis as a Tool for HTI Parameters Estimation, EAGE 65th Conference and Technical Exhibition, Stavanger.

Mushin I.A., Makarov, V.V., Kozlov E.A., and Lowrie A., 2000. Structural-Formational Interpretation Tools for Seismic Stratigraphy. Geophysical Prospecting, 48, 953-981.

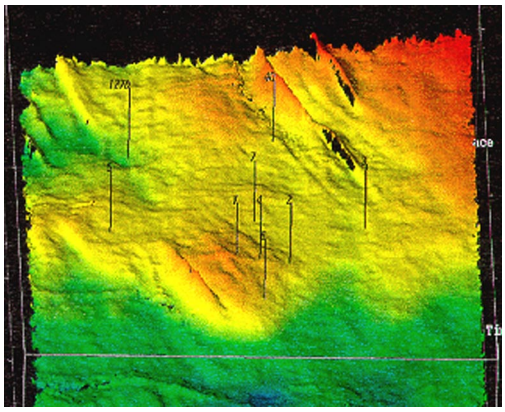

Fig. 1. Stereometric image of the target interval bottom. The oil bearing anticline is localized in the middle of the image. Wells 1, 2, 4, 6 are productive, while other wells are not.

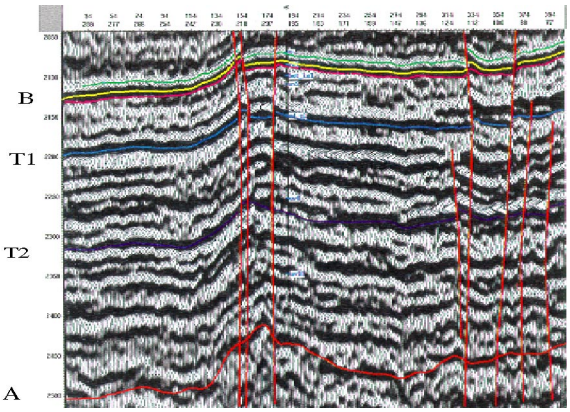

Fig. 2. A typical depth migrated seismic section converted to time domain to ease azimuthal velocity and AVO analysis.

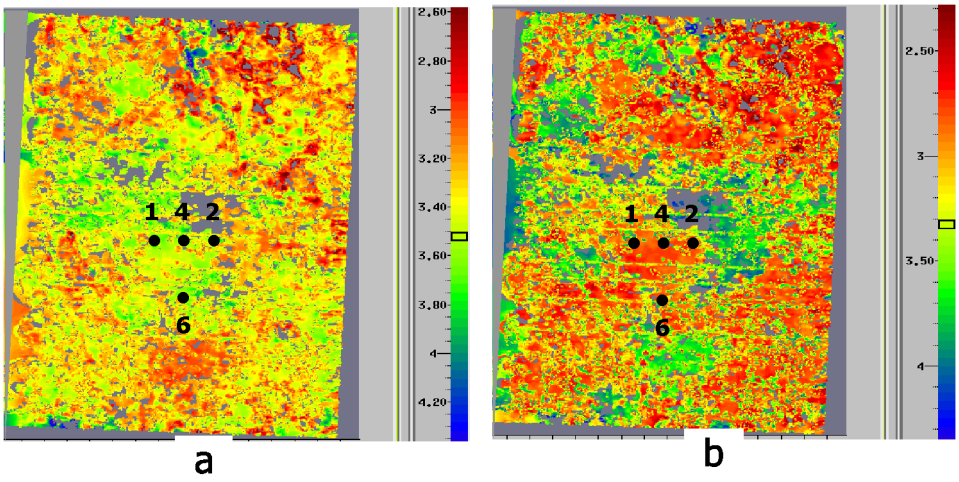

Fig. 3. Interval P-wave velocity for the interval between seismic horizons B and T2 calculated assuming horizontal transverse isotropy (HTI) for directions normal (**a**) and parallel (**b**) to the HTI axis of symmetry.

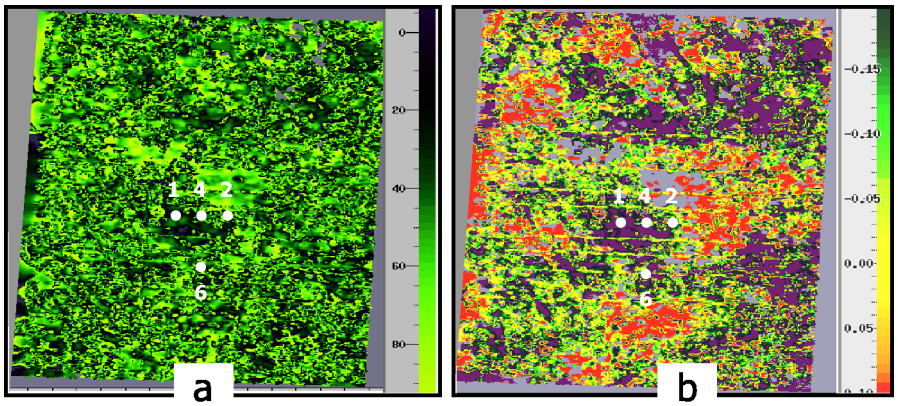

Fig. 4. Direction of the HTI axis of symmetry (**a**), and Thomsen HTI anisotropy coefficient δ defined with respect to vertical (**b**). Note high anistrophy in the area of high productivity ($|\delta|$ about 0.18). Note also N-S orientation of the axis of symmetry in the high productivity area and W-E orientation just to the North of the area.

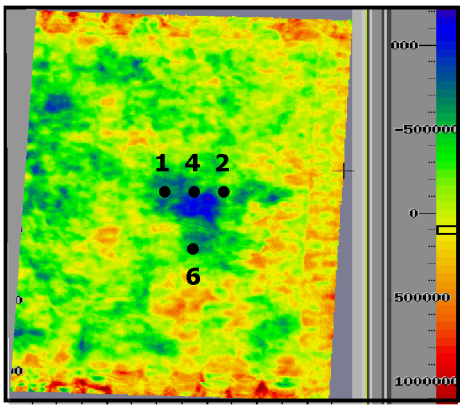

Fig. 5. Map of the difference between AVO gradients in directions normal and parallel to the HTI axis of symmetry which is a measure of anisotropy coefficient δ.

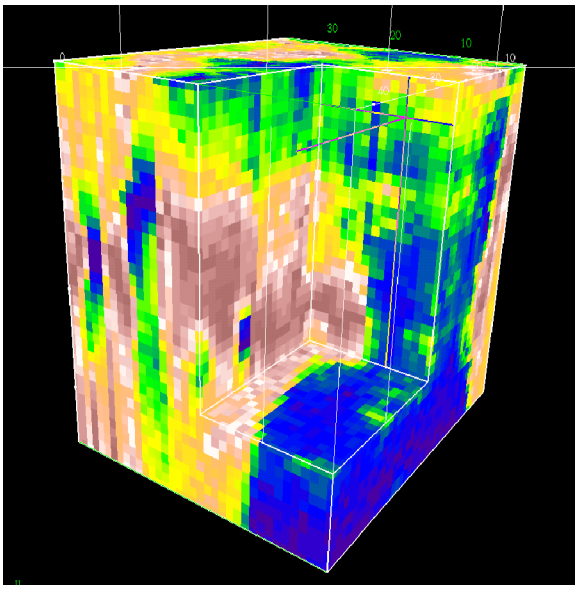

Fig. 6. Cube of average stress variations $\Delta\sigma = \sigma - \Sigma$, where Σ is the lithostatic pressure defined by horizontal averaging of the confining stress σ values over each depth slice.

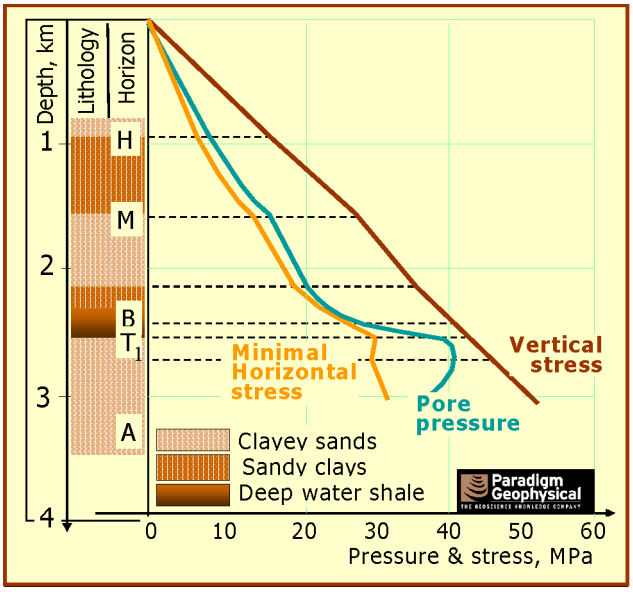

Fig. 7. Vertical profiles of maximum pore pressure and lithostatic stress components - vertical and minimum horizontal. Note maximum pore pressure exceeding the minimum horizontal stress and sharp increase of the maximum pore pressure in the target interval.

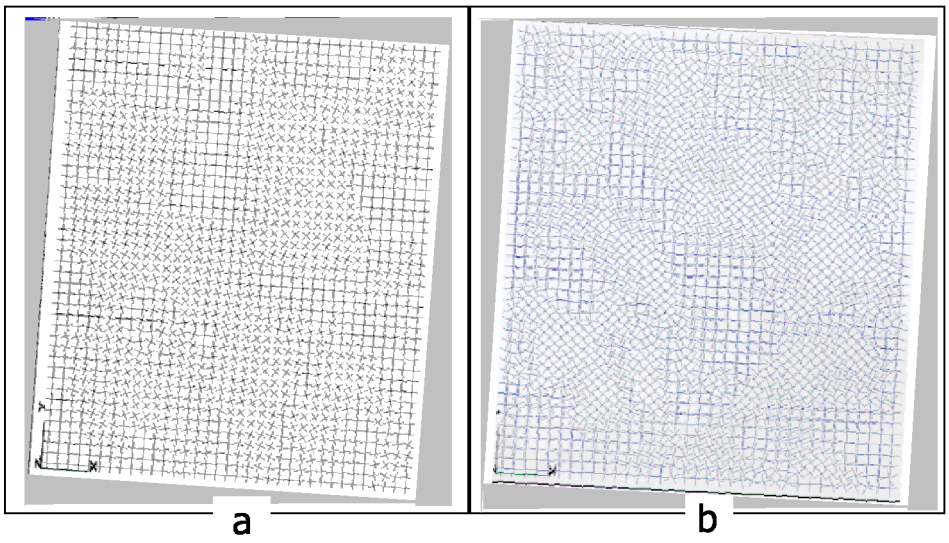

Fig. 8. Orientations of the minimum horizontal stress in the Cretaciuois rocks above the horizon B **(a)** and in the target interval between horizons B and T2 **(b)**. Note general consistence between strikes of main faults (**Figure1**), orientations of the HTI axis of symmetry (**Figure 4a**), and orientations of minimum horizontal stresses in the target interval, **Figure 8b.**

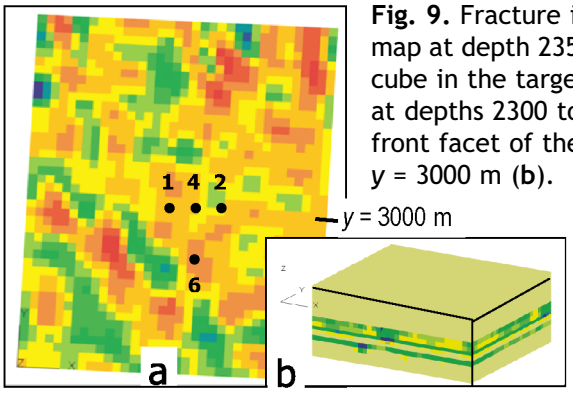

Fig. 9. Fracture intensity map at depth 2350 m (**a**) and cube in the target interval at depths 2300 to 2400 m, front facet of the cube at *y* = 3000 m (**b**).

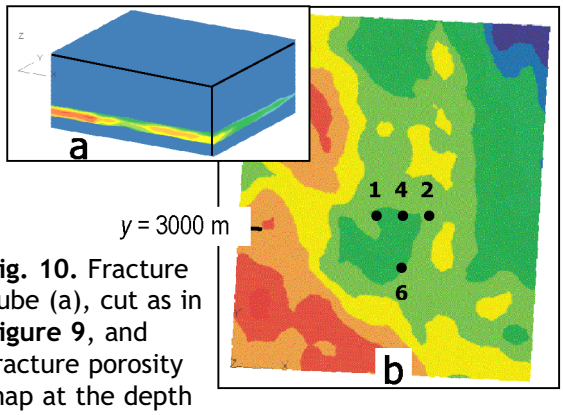

Fig. 10. Fracture cube (a), cut as in **Figure 9**, and fracture porosity map at the depth of 2350 m (**b**).